Direct Active and Reactive Power Control of Three-Phase Inverter for AC Motor Drives With Small DC-Link Capacitors Fed by Single-Phase Diode Rectifier

ByungGil Kwak, Jeong-Heum Um, and Jul-Ki Seok, *Senior Member, IEEE*

***Abstract*—This paper proposes a power controller used for three-phase inverters with small dc-link capacitors fed by a single-phase diode rectifier. The effect of the reactive power was investigated based on a power flow analysis between a dc-link and three-phase inverter. These results enable the development of a direct active/reactive power controller in discrete time instead of adopting a classical proportional-integral (PI)-type current regulator, which directly leverages the total power flow of the system. A suitable reactive power selection method was presented to improve the overall system efficiency. The command voltage vector at each discrete time step can be simply and intuitively determined by an inverter power without requiring motor current-regulating PI gains and additional control functions. The proposed controller regulates an average motor velocity/airgap torque while simultaneously shaping a grid-side current with a high power factor and low harmonics to meet IEC61000-3-2 requirements. The proposed structure can be applied to three-phase inverters for a broad family of ac motors, such as induction and permanent magnet synchronous motors.**

***Index Terms*—Ac motor drives, direct active/reactive power controller (DPQC), single-phase diode rectifier, three-phase inverters with small dc-link capacitors.**

I. Introduction

DC-LINK electrolytic capacitors represent a limiting factor of three-phase voltage source inverters because of their lower power density and uncertain/time-dependent lifetime [1]–[3]. In particular, when the inverter is fed through a diode rectifier, a power factor correction (PFC) or passive filter circuit is required to meet IEC61000-3-2 harmonic regulations [4]. In addition, an initial charging circuit is necessary to limit excessive inrush currents [5]. These additional circuits result in a substantial increase in cost and loss of power density.

To solve these problems, greater focus has been recently given to a three-phase inverter with small dc-link capacitors fed by a single-phase diode rectifier that ensures longer cyclic operational periods, long-term reliability, and greater whole-system power density [6]–[11]. Because a small capacitance provides a clear footprint of the grid-side voltage to the dc-link in this system, an average motor velocity can be regulated while simultaneously shaping a nearly sinusoidal grid-side current.

Despite the aforementioned advantages, the development of inverters with small dc-link capacitors has not been straightforward because the periodic dc-link voltage drops result in considerable challenges in system control. The dc-link voltage with a double-grid frequency propagates to the ac motor because the motor terminal voltages are synthesized with respect to the swinging dc-link voltage. This fluctuation causes an oscillation of the motor airgap torque and velocity. Therefore, the application of this inverter should be limited to the industrial areas that can allow these fluctuations. Recently, small dc-link capacitor inverters have been applied to compressor-installed motor drives and heating-ventilating-air-conditioning (HVAC) applications [6], [7]. These cost and efficiency sensitive applications are typically characterized by sluggish dynamics, nearly constant velocity operation, and rare regeneration, which must be accounted for in the small dc-link capacitor inverter controller design [12], [13].

The conventional small dc-link capacitor inverter control strategies were developed to perform simultaneously grid current shaping and motor control based on a PI-type current regulator [6]–[10], which is a well-developed technique for classical inverters with large electrolytic capacitors. These control approaches are very efficient and powerful, but often overlook the fact that instantaneous current control is not straightforward due to frequent dc-link voltage drops. The inverter control strategy becomes more complicated because it requires an extra control function and tuning gains, which should be selected carefully based on the complex tradeoff between the drive stability and control dynamics. Thus, the current regulator leaves the motor current very close to an open-loop state because the current

Manuscript received December 23, 2018; revised February 18, 2019 and April 22, 2019; accepted April 22, 2019. Date of publication May 5, 2019; date of current version June 29, 2019. Paper 2018-IDC-1321.R2, presented at the 2018 IEEE/IAS Industrial and Commercial Power Systems Technical Conference, Portland, OR, USA, Sep. 23–27, and approved for publication in the IEEE TRANSACTIONS ON INDUSTRY APPLICATIONS by the Industrial Drives Committee of the IEEE Industry Applications Society. This research was supported by Basic Science Research Program through the National Research Foundation of Korea (NRF) funded by the Ministry of Science and ICT (NRF-2017R1A2B4001787). *(Corresponding author: Jul-Ki Seok.)*

B. Kwak is with Aerospace Mechanical R&D Center, Hanwha Aerospace Corp., Asan-city 31409, South Korea (e-mail: kwak_bg@hanwha.com).

J.-H. Um and J. K. Seok are with the School of Electrical Engineering, Yeungnam University, Gyeongbuk 38541, South Korea (e-mail: zxshtw12@ynu.ac.kr; doljk@ynu.ac.kr).

Color versions of one or more of the figures in this paper are available online at http://ieeexplore.ieee.org.

Digital Object Identifier 10.1109/TIA.2019.2915061

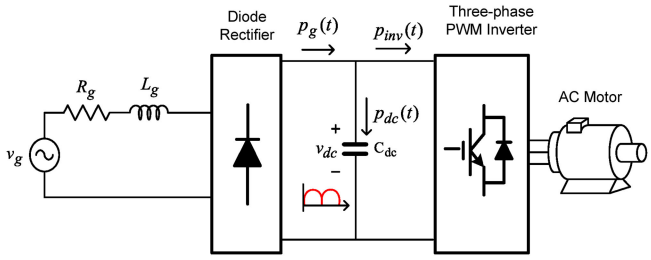

Fig. 1. Circuit configuration of three-phase inverter with small dc-link capacitor fed by a single-phase diode rectifier.

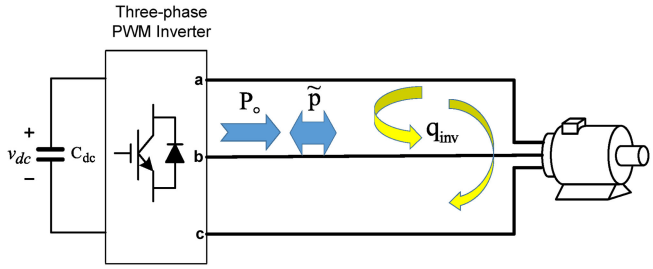

Fig. 2. Instantaneous active and reactive power flow in a three-phase circuit.

ripple is inherent in this system. Consequently, selecting a current command or controller gains would be a daunting task. Moreover, dealing with a reactive power of the motor has yet to be reported. If this is not considered by a designed controller, system efficiency may be lost. In these approaches, the range of applicable motors is limited to permanent magnet (PM) type motors.

The main contribution of this paper is the development and implementation of a direct active and reactive power controller (DPQC) for small dc-link film capacitor inverters fed by single-phase diode rectifiers. Instead focusing on conventional motor current regulation, a power-level controller was designed in the discrete-time domain, where the resulting control actions can be determined analytically. This creates the ability to track an instantaneous active and reactive power command of the motor and shape a sinusoidal grid current simultaneously. An inverter output voltage at every sampling instant can be easily calculated without requiring any complicated decision algorithm and control gains. In this paper, a motor reactive power command selection rule is proposed to improve the system efficiency and reduce the grid current with respect to a given active power demand of the motor. The unified control approach can be applied to a wide range of ac motors, such as PM and induction motors (IMs).

II. Power Flow of Small DC-Link Capacitor Inverter

Fig. 1 shows a circuit configuration of a three-phase inverter with small dc-link capacitors fed by a single-phase diode rectifier, where v_g is the ac grid voltage, R_g/L_g represents the input resistance/inductance, and p_g is the rectified active power. In addition, $v_{\rm dc}/C_{\rm dc}$ denotes the dc-link voltage/capacitance, $p_{\rm dc}$ is the dc-link active power, and $p_{\rm inv}$ is the instantaneous active power supplied to the inverter from the dc-link.

In this system, the dc-link voltage has considerable fluctuation with a double-grid frequency. Therefore, the inverter operation for motor control is not trivial due to the periodical absence of the available dc-link voltage. Moreover, the grid-side current should meet IEC61002-3-2 harmonic regulation without any input filers and PFC circuits.

A. Power Theory in Three-Phase Inverter

Neglecting the power loss of the inverter, the instantaneous active and reactive power supplied to the inverter from the dc-link can be obtained as

$$p_{\rm inv}(t) = \frac{3}{2}{\rm Re}\left(\mathbf{v}_{dqs}\mathbf{i}^{\bullet}_{dqs}\right) \tag{1}$$

$$q_{\rm inv}(t) = \frac{3}{2}{\rm Im}\left(\mathbf{v}_{dqs}\mathbf{i}^{\bullet}_{dqs}\right) \tag{2}$$

where $\mathbf{v}_{dqs}$ and $\mathbf{i}_{dqs}$ are the d–q axis motor phase voltage and current vector in the arbitrary reference frame, respectively, and $\bullet$ denotes the complex conjugate.

The instantaneous active power can be expressed as

$$p_{\rm inv}(t) = P_\circ + \tilde{p} \tag{3}$$

where $P_\circ$ represents a dc value of the instantaneous real power that is transferred from the dc-link to the motor, and $\tilde{p}$ indicates a ripple component exchanged between the dc-link and the motor [13], [14]. By contrast, if the grid-side current is in phase with the grid-side source voltage, $q_{\rm inv}(t)$ is trapped in each phase and is exchanged between each phase of the motor. Hence, $q_{\rm inv}(t)$ could be adjusted to minimize the motor phase current without affecting the real power flow, as shown in Fig. 2. Thus, a desirable reactive power can minimize a motor stator current for a given active power demand, which naturally leads to a reduced grid-side current magnitude, as the grid supplies the main power to the inverter and motor. In other words, selecting a suitable reactive power contributes to more efficient operation of the small dc-link capacitor inverter, which is essentially required for HVAC applications. This approach provides a different level of insight into the control framework for the three-phase inverter with small dc-link capacitors.

B. Direct Active/Reactive Control for Small DC-Link Capacitor Inverters

In this paper, a DPQC is designed in discrete time to regulate the grid-side current and to track the changes in motor power simultaneously. The proposed controller improves the system efficiency with reactive power control as compared to existing PI-type current regulator-based control schemes.

Neglecting the inverter and motor losses, the instantaneous inverter active power can be approximated as [6], [7]

$$p_{\rm inv}(t) \cong p_g(t) - p_{\rm dc}(t) \cong V_g I_g \sin^2\theta_g - \frac{1}{2}\omega_g C_{\rm dc} V_g^2 \sin 2\theta_g$$
$$\cong 2\omega_{rm}\overline{T}_e \sin^2\theta_g \tag{4}$$

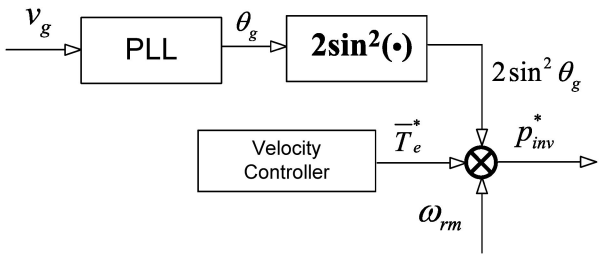

Fig. 3. Inverter active power command generation.

where V_g/I_g is the peak value of the grid voltage and current, respectively, θ_g is the grid voltage phase angle obtained from a phase-locked loop, and ω_g is the angular velocity of the grid voltage. In addition, ω_{rm} denotes the mechanical angular velocity of the motor and $\overline{T}_e$ indicates the average value of the motor air-gap torque. This equation implies that the active power in a small dc-link capacitor inverter should be regulated according to the dc-link voltage fluctuations with the double-grid frequency. Therefore, the inverter active power command can be calculated as

$$p_{\rm inv}^*(t) = 2\omega_{rm}\overline{T}_e^*\sin^2\theta_g. \tag{5}$$

The inverter active power command generation is represented as a block diagram in Fig. 3.

In order to form the proposed DPQC law, the following power differential equation from (1) and (2) can be written as

$$\dot{p}_{\rm inv} = \frac{3}{2}\left(\dot{v}_{ds}i_{ds} + v_{ds}\dot{i}_{ds} + \dot{v}_{qs}i_{qs} + v_{qs}\dot{i}_{qs}\right) \tag{6a}$$

$$\dot{q}_{\rm inv} = \frac{3}{2}\left(\dot{v}_{qs}i_{ds} + v_{qs}\dot{i}_{ds} - \dot{v}_{ds}i_{qs} - v_{ds}\dot{i}_{qs}\right) \tag{6b}$$

where the stator and rotor variables are expressed in an arbitrary reference frame.

The rate of change in the inverter voltage and current can be developed over a pulsewidth modulation (PWM) period, T_s, such that

$$\Delta\mathbf{v}_{dqs}(k) = \frac{\mathbf{v}_{dqs}^*(k) - \mathbf{v}_{dqs}(k)}{T_s} \tag{7a}$$

$$\Delta\mathbf{i}_{dqs}(k) = \frac{\mathbf{i}_{dqs}^*(k) - \mathbf{i}_{dqs}(k)}{T_s} \tag{7b}$$

where superscript "$*$" represents the corresponding command variables in this paper.

Combining (6) and (7) gives

$$\Delta p_{\rm inv}(k) = \frac{3}{2}\begin{pmatrix}\left(\frac{v_{ds}^*(k)-v_{ds}(k)}{T_s}\right)i_{ds} + v_{ds}\left(\frac{i_{ds}^*(k)-i_{ds}(k)}{T_s}\right)\\ +\left(\frac{v_{qs}^*(k)-v_{qs}(k)}{T_s}\right)i_{qs} + v_{qs}\left(\frac{i_{qs}^*(k)-i_{qs}(k)}{T_s}\right)\end{pmatrix}. \tag{8a}$$

On the other hand, the inverter reactive power command can be constructed from the conventional maximum torque per ampere (MTPA) (salient PM motors) or the rated flux linkage (IMs) information. Thus, the reactive power change in discrete time is

$$\Delta q_{\rm inv}(k) = \frac{3}{2}\begin{pmatrix}\left(\frac{v_{qs}^*(k)-v_{qs}(k)}{T_s}\right)i_{ds} + v_{qs}\left(\frac{i_{ds}^*(k)-i_{ds}(k)}{T_s}\right)\\ -\left(\frac{v_{ds}^*(k)-v_{ds}(k)}{T_s}\right)i_{qs} - v_{ds}\left(\frac{i_{qs}^*(k)-i_{qs}(k)}{T_s}\right)\end{pmatrix}. \tag{8b}$$

As described in Section III, the proposed power control scheme turns out to be applicable to any type of ac motor such as PM synchronous and IMs.

III. DPQC Design for AC Motors

A. DPQC Design for Salient PM Synchronous Motors

The rate of change in the stator current of salient PM synchronous motors can be obtained from the voltage equation in [15]

$$\frac{i_{ds}^{r*}(k) - i_{ds}^r(k)}{T_s} = \frac{1}{L_d}\left(v_{ds}^{r*}(k) - R_s i_{ds}^r(k) + \omega_r L_q i_{qs}^r(k)\right) \tag{9a}$$

$$\frac{i_{qs}^{r*}(k) - i_{qs}^r(k)}{T_s} = \frac{1}{L_q}\left(v_{qs}^{r*}(k) - R_s i_{qs}^r(k) - \omega_r(L_d i_{ds}^r(k) + \lambda_{\rm pm})\right) \tag{9b}$$

where $\mathbf{v}_{dqs}^r$ and $\mathbf{i}_{dqs}^r$ are the stator voltage and current vector in the rotor reference frame, respectively, R_s is the stator resistance, ω_r is the electrical rotor angular velocity, $\lambda_{\rm pm}$ is the flux linkage of the PM, and $L_{\rm dq}$ denotes the *d–q* axis stator inductance.

Substituting (9) into (8) yields the inverter power, which is given as

$$\Delta p_{\rm inv}(k) = \frac{3}{2}\left(A_1 v_{ds}^{r*}(k) + A_2 v_{qs}^{r*}(k) + A_3 v_{ds}^r(k) + A_4 v_{qs}^r(k)\right) \tag{10a}$$

$$\Delta q_{\rm inv}(k) = \frac{3}{2}\left(B_1 v_{ds}^{r*}(k) + B_2 v_{qs}^{r*}(k) + B_3 v_{ds}^r(k) + B_4 v_{qs}^r(k)\right) \tag{10b}$$

where the coefficients A_1, A_2, A_3, A_4, B_1, B_2, B_3, and B_4 are constant values whose mathematical expression is presented in Appendix A.

A voltage command in the next sampling time can be uniquely obtained from (7) and (10) as a function of the inverter power

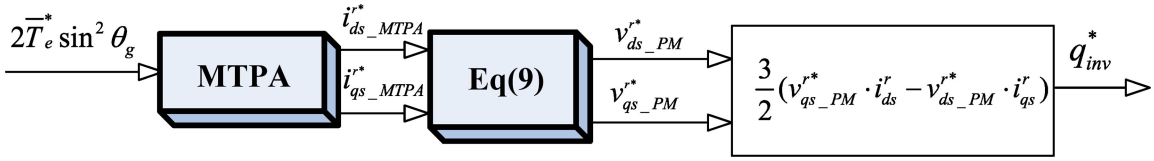

Fig. 4. Reactive power command for salient PM motors.

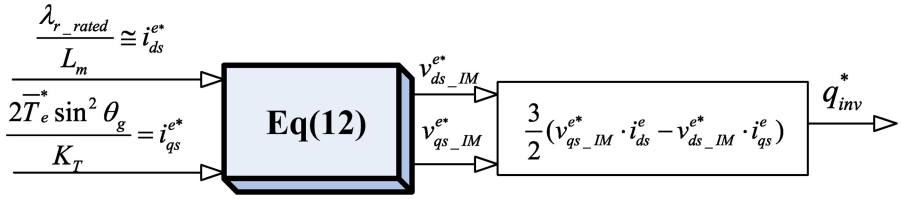

Fig. 5. Reactive power command for RFO-controlled IMs.

and the voltage/current value of the *k*th sampling time

$$v_{ds}^{r*}(k) = \frac{2}{3}\left(\frac{B_2}{A_1B_2 - A_2B_1}\right)\Delta p_{\mathrm{inv}}(k) - \frac{2}{3}\left(\frac{A_2}{A_1B_2 - A_2B_1}\right)\Delta q_{\mathrm{inv}}(k) - \left(\frac{A_3B_2 - A_2B_3}{A_1B_2 - A_2B_1}\right)v_{ds}^{r}(k) - \left(\frac{A_4B_2 - A_2B_4}{A_1B_2 - A_2B_1}\right)v_{qs}^{r}(k) \tag{11a}$$

$$v_{qs}^{r*}(k) = \frac{2}{3}\frac{1}{B_2}\Delta q_{\mathrm{inv}}(k) - \frac{B_1}{B_2}v_{ds}^{r*}(k) - \frac{B_3}{B_2}v_{ds}^{r}(k) - \frac{B_4}{B_2}v_{qs}^{r}(k). \tag{11b}$$

The reactive power command of salient PM motors can be simply obtained using the MTPA information, as shown in Fig. 4.

B. DPQC Design for IMs

The rate of change in the stator current can be obtained from the voltage equation of induction motors in [15] as

$$\frac{i_{ds}^{e*}(k) - i_{ds}^{e}(k)}{T_s} = \frac{1}{L_\sigma}\left(v_{ds}^{e*}(k) - R_s i_{ds}^{e}(k) + \omega_e L_\sigma i_{qs}^{e}(k)\right) \tag{12a}$$

$$\frac{i_{\mathrm{qs}}^{e*}(k) - i_{\mathrm{qs}}^{e}(k)}{T_s} = \frac{1}{L_\sigma}\left(v_{\mathrm{qs}}^{e*}(k) - R_s i_{\mathrm{qs}}^{e}(k) - \omega_e L_s i_{\mathrm{ds}}^{e}(k)\right) \tag{12b}$$

where $\mathbf{v}_{dqs}^{e}$ and $\mathbf{i}_{dqs}^{e}$ are the stator voltage and current vector in the synchronously rotating reference frame, respectively, ω_e is the electrical synchronous angular velocity, L_s indicates the stator inductance, and L_σ denotes the stator transient inductance.

Substituting (12) into (8) becomes

$$\Delta p_{\mathrm{inv}}(k) = \frac{3}{2}\left(C_1 v_{ds}^{e*}(k) + C_2 v_{qs}^{e*}(k) + C_3 v_{ds}^{e}(k) + C_4 v_{qs}^{e}(k)\right) \tag{13a}$$

$$\Delta q_{\mathrm{inv}}(k) = \frac{3}{2}\left(D_1 v_{ds}^{e*}(k) + D_2 v_{qs}^{e*}(k) + D_3 v_{ds}^{e}(k) + D_4 v_{qs}^{e}(k)\right) \tag{13b}$$

where the coefficients C_1, C_2, C_3, C_4, D_1, D_2, D_3, and D_4 are constant values whose mathematical expression is described in Appendix B.

A voltage command in the next sampling time can be uniquely obtained as

$$v_{ds}^{e*}(k) = \frac{2}{3}\left(\frac{D_2}{C_1D_2 - C_2D_1}\right)\Delta p_{\mathrm{inv}}(k) - \frac{2}{3}\left(\frac{C_2}{C_1D_2 - C_2D_1}\right)\Delta q_{\mathrm{inv}}(k) - \left(\frac{C_3D_2 - C_2D_3}{C_1D_2 - C_2D_1}\right)v_{ds}^{e}(k) - \left(\frac{C_4D_2 - C_2D_4}{C_1D_2 - C_2D_1}\right)v_{qs}^{e}(k) \tag{14a}$$

$$v_{qs}^{e*}(k) = \frac{2}{3}\frac{1}{D_2}\Delta q_{\mathrm{inv}}(k) - \frac{D_1}{D_2}v_{ds}^{e*}(k) - \frac{D_3}{D_2}v_{ds}^{e}(k) - \frac{D_4}{D_2}v_{qs}^{e}(k). \tag{14b}$$

The reactive power command of rotor-flux-oriented (RFO) controlled IMs can be obtained using the rated rotor flux linkage information $\lambda_{r\_\mathrm{rated}}$, as shown in Fig. 5, where L_m is the magnetizing inductance and K_T indicates the torque constant.

The HVAC systems or compressor-installed motor drives perform rated or high speed rotating motions under non-zero loads. Thus, it would be reasonable to investigate the singularity of $\begin{bmatrix} A_1 & A_2 \\ B_1 & B_2 \end{bmatrix}$ and $\begin{bmatrix} C_1 & C_2 \\ D_1 & D_2 \end{bmatrix}$ in (10) and (13) at this main operating

TABLE I
RATINGS AND KNOWN PARAMETERS OF 900 W SALIENT PM MOTOR

Ratings and Parameters	Value	Unit
Rated torque	2.9	Nm
L_d	8.5	mH
L_q	20.2	mH
λ_{pm}	0.115	Wb

TABLE II
RATINGS AND KNOWN PARAMETERS OF 1.5 kW IM UNDER TEST

Ratings and Parameters	Value	Unit
Rated torque	9.7	Nm
R_s / R_r @25°C	2.47 / 0.7	Ω
L_m / L_σ	134 / 12.6	mH

condition. In this regard, the motor angular velocity and the d–q axis voltage/current of (A1), (A2), (B1), (B2), (C1), (C2), (D1), and (D2) have a non-zero value under the above condition, which implies that (10) and (13) are solvable.

The designed DPQC operates instantaneously and is responsible for balancing the power demand and supply of ac motors. Fig. 6 shows how the voltage vector can be determined at every sampling instant in the d–q voltage plane under the condition of a different dc-link voltage drop. The proposed DPQC provides a feasible and unique inverter voltage command without requiring any complicated mode transition schemes and gain selections. The command voltage vector can be chosen in a similar manner for non-salient PM motors.

Fig. 7 shows the overall control block diagram, which has a streamlined structure and the proposed idea is intuitively understood, where the Overmodulation block represents an overmodulation function. The proposed approach shows a control partitioning that can partition an inverter power into an active power that is responsible for regulation of the average velocity and grid-side current, and a reactive power for efficiency control. Note that the successful command voltage selection of (11) and (14) can be achieved provided no drift of the motor parameter exists. However, in practice, this is not always the case, and the motor parameters should be estimated and updated.

IV. EXPERIMENTAL RESULTS

The basic feasibility of the proposed DPQC method was verified on a 900 W salient PM motor and 1.5 kW IM, as given in Tables I and II. The PWM voltage source inverter inverter used here consists of 5 kHz switching insulated gate bipolar transistor modules. Two-phase currents were sampled with a rate of 100 μs. The dc-link film capacitor was selected as 5 μF and the velocity control bandwidth was set to 10 Hz. A filter capacitance of the dc-link side is around 1000 μF in the

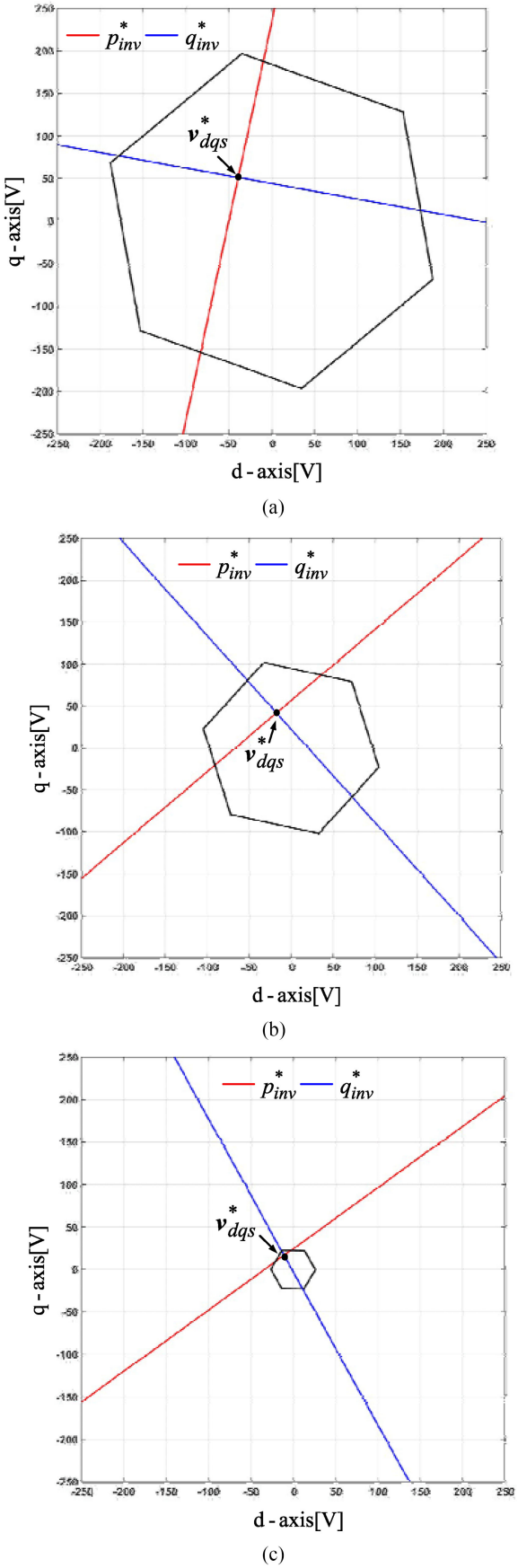

Fig. 6. Voltage command vector selection under the dc-link voltage oscillation condition. (a) V_{dc} = 300 V. (b) V_{dc} = 160 V. (c) V_{dc} = 40 V.

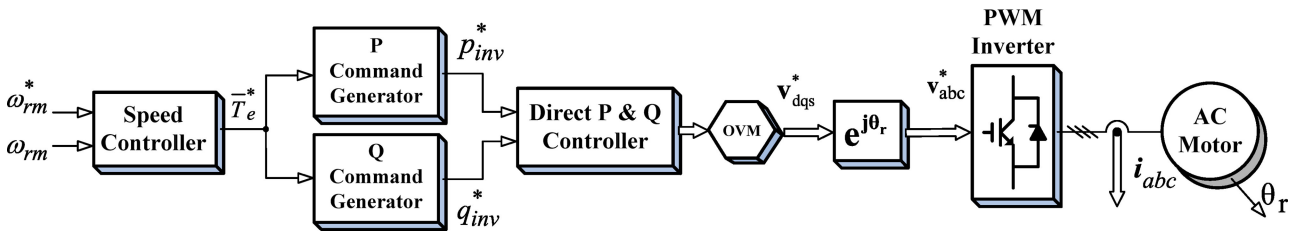

Fig. 7. Overall control block diagram.

conventional 1 kW general-purpose inverters fed by the single-phase diode rectifier [7]. An additional mechanical ripples or oscillations from a load side gives little impact to proposed direct active and reactive power control because of the low-velocity control bandwidth.

It is interesting to speculate on how the selection of the dc-link capacitance affects the quality of the grid-side current and motor airgap torque. When the dc-link capacitance is ever-increasing, the grid-side current is more distorted with a higher total harmonic distortion for a given grid-side line inductance. On the other hand, for a small dc capacitance, the high switching frequency ripple continues to increase due to the lack of the filtering capacitance. The quality of the motor torque is not much affected by the value of the dc-link capacitance because the proposed controller is responsible for motor control with the given dc-link voltage. In this paper, the dc-link capacitance was selected by the simulation and experimental tests.

Fig. 8(a) presents a steady-state test result for the salient PM motor, where the inverter output voltage magnitude/limit, active power command/controlled active power, and reactive power command/controlled reactive power are illustrated from top to bottom. In this test, the grid voltage was set to 220 Vrms and the motor drive was operated at a half-rated torque and at 1600 r/min. The active and reactive power were well-regulated even under the available dc-link vanishing conditions.

To examine the grid-side control performance, as shown in Fig. 8(b), the measured d–q axis stator current in the synchronous coordinate and the grid voltage/grid current are depicted from top to bottom. As observed from the grid voltage and current waveform, the current is quite sinusoidal and gives a high power factor (>96.5%) with the 5 μF capacitor-inverter. Because the inverter power is well-regulated, the motor phase currents are also well-behaved to generate the motor power without the PI-type current regulator. Fig. 8(c) shows the measured motor velocity, the generated torque command, and the measured d–q axis stator current in the synchronous coordinate from top to bottom. In terms of averages, the rotor velocity tracks the 1600 r/min velocity command well and the nearly half-rated torque command is generated to regulate the motor velocity.

Fig. 9 shows the grid current harmonics along with IEC61000-3-2 Class A standard. The proposed DPQC can provide new opportunities in a small dc-link capacitor inverter fed by single-phase diode-bridge rectifiers, which experiences frequent and deep dc-bus voltage drops.

Fig. 10(a) shows the experimental results of the IM at 20% of the rated torque and at 1500 r/min, where the measured d–q axis

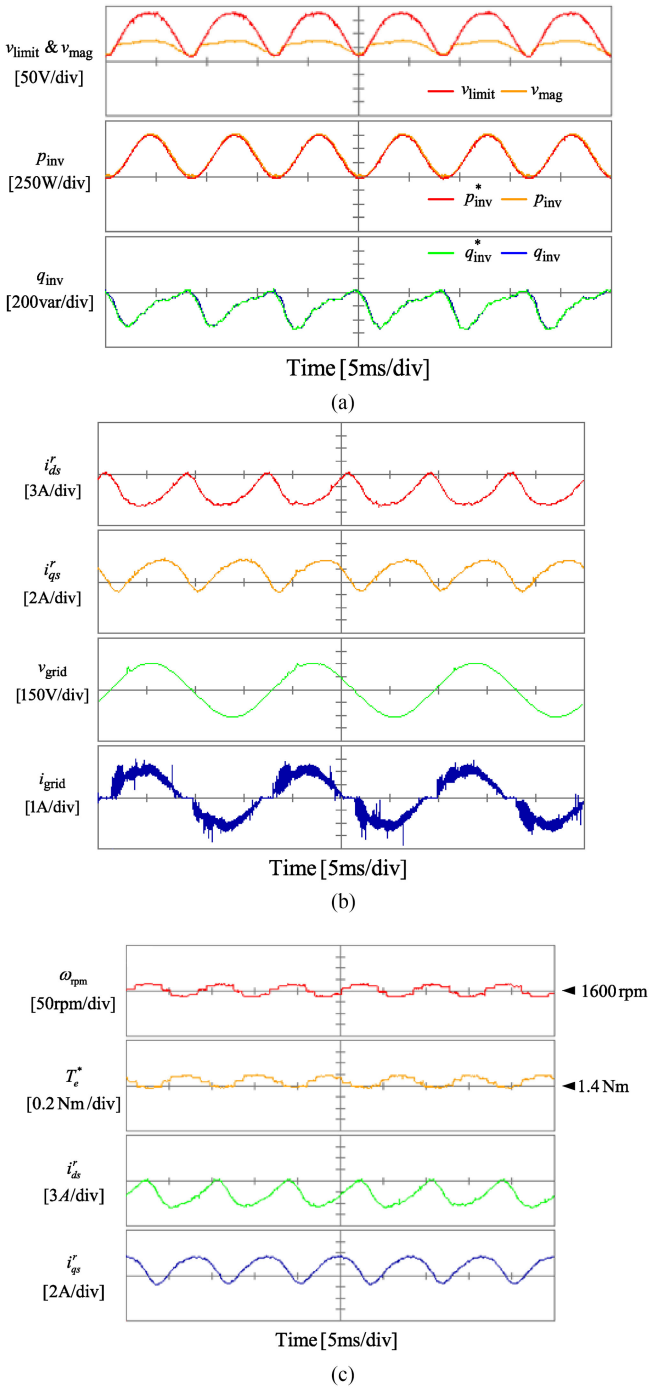

Fig. 8. Experimental results of the proposed controller for the salient PM motor.

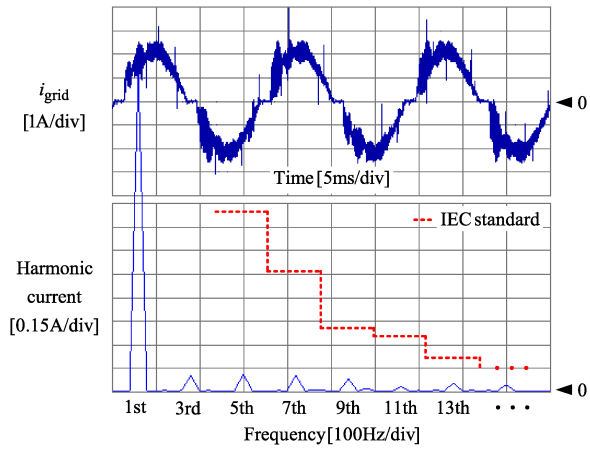

Fig. 9. Harmonic analysis of the grid current for the salient PM motor.

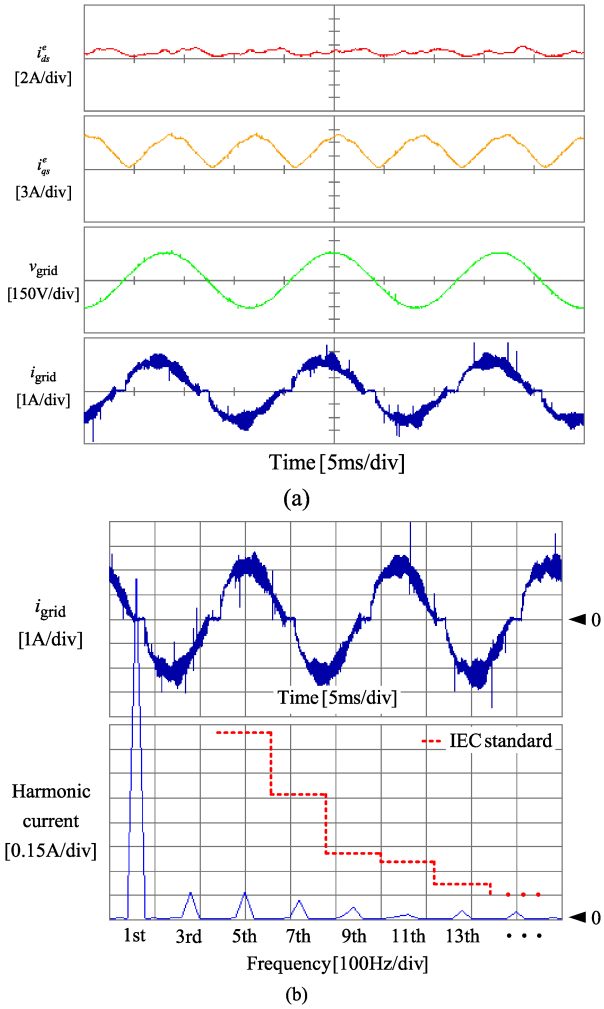

Fig. 10. Experimental results of the proposed controller for the IM.

current in the synchronous coordinate and grid voltage/current are illustrated from top to bottom. The motor currents fluctuate with the double-grid frequency to regulate the motor air-gap torque. The grid current is nearly sinusoidal without the PFC circuit and bulky input low-pass filters. According to Fig. 10(b), the grid current harmonics comply with IEC61000-3-2 Class A standard. To the best of our knowledge, the application of the

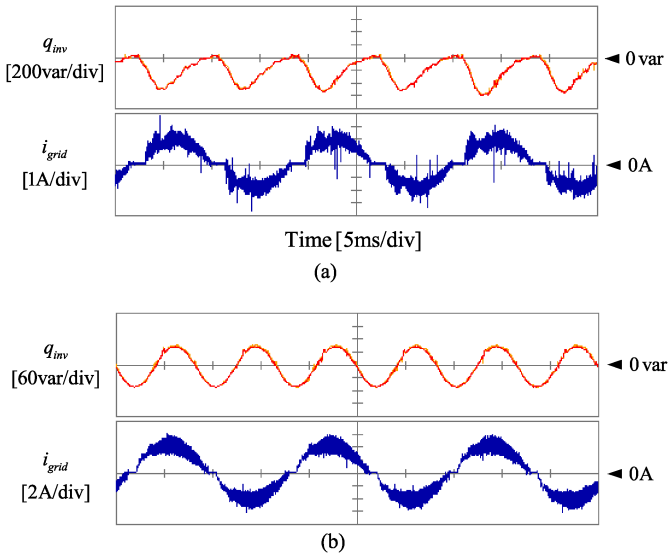

Fig. 11. Comparison test results for different reactive power command selection.

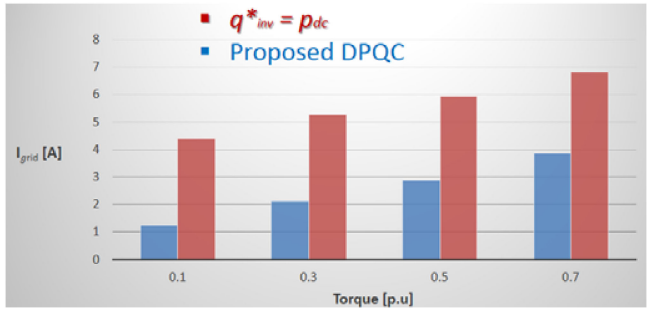

Fig. 12. Comparison test results of grid current magnitude for each reactive power command selection with load torque.

small dc-link capacitor inverter to IMs has not been previously reported in the existing literature.

Two tests were conducted to examine how the proposed reactive power control affects system efficiency. Fig. 11(a) shows the controlled reactive power and grid-side current of the proposed controller under the tested salient PM motor. The amplitude of the grid-side current reached 2 A. The same test was performed under the identical active power demand with respect to a reactive power command, as shown in Fig. 11(b). Here, the command was selected as $p_{\rm dc}$ of (4), which is quite smaller than that of the proposed method. The grid current was reduced by 56% compared to that of the selected reactive power command. The proposed control scheme may not be optimal but is practically effective/simple compared to existing control methods for the reactive power manipulation.

To assess how much the grid current is reduced with different load torque levels, the grid current amplitudes were compared with each other as shown in Fig. 12. These results clearly show that the proposed DPQC is effective at making the small dc-link inverter system more efficient. This can be considered a major improvement by efficiency-sensitive HVAC drive makers.

V. Conclusion

This paper was the first to report a genuine direct active and reactive power control method for small dc-link capacitor inverters fed by single-phase diode rectifiers. With the power flow analysis, it was found that a suitable selection of the reactive power can improve the system efficiency and reduce the grid-side current with respect to a given active power demand of the motor. The command inverter output voltage can be determined simply by calculating the intersection of the active and reactive power in the *d–q* voltage plane. The proposed structure leads to a control partitioning for active and reactive power to regulate the average motor velocity and improve the system efficiency while simultaneously shaping the grid-side current. The single control law is maintained without requiring any complicated mode transition schemes and gain selections.

Appendix A

The coefficients used in (11a) and (11b) are

$$A_1 = \frac{i^r_{ds}(k)}{T_s} + \frac{v^r_{ds}(k)}{L_d} \tag{A1}$$

$$A_2 = \frac{i^r_{qs}(k)}{T_s} + \frac{v^r_{qs}(k)}{L_q} \tag{A2}$$

$$A_3 = -\frac{i^r_{ds}(k)}{T_s} - \frac{R_s i^r_{ds}(k)}{L_d} + \frac{\omega_r L_q i^r_{qs}(k)}{L_d} \tag{A3}$$

$$A_4 = -\frac{i^r_{qs}(k)}{T_s} - \frac{R_s i^r_{qs}(k)}{L_q} - \frac{\omega_r L_d i^r_{ds}(k)}{L_q} - \frac{\omega_r \lambda_{\rm pm}}{L_q} \tag{A4}$$

$$B_1 = -\frac{i^r_{qs}(k)}{T_s} + \frac{v^r_{qs}(k)}{L_d} \tag{A5}$$

$$B_2 = \frac{i^r_{ds}(k)}{T_s} - \frac{v^r_{ds}(k)}{L_q} \tag{A6}$$

$$B_3 = \frac{i^r_{qs}(k)}{T_s} + \frac{R_s i^r_{qs}(k)}{L_q} + \frac{\omega_r L_d i^r_{ds}(k)}{L_q} + \frac{\omega_r \lambda_{\rm pm}}{L_q} \tag{A7}$$

$$B_4 = -\frac{i^r_{ds}(k)}{T_s} - \frac{R_s i^r_{ds}(k)}{L_d} + \frac{\omega_r L_q i^r_{qs}(k)}{L_d}. \tag{A8}$$

Appendix B

$$C_1 = \frac{i^e_{ds}(k)}{T_s} + \frac{v^e_{ds}(k)}{L_\sigma} \tag{B1}$$

$$C_2 = \frac{i^e_{qs}(k)}{T_s} + \frac{v^e_{qs}(k)}{L_\sigma} \tag{B2}$$

$$C_3 = -\frac{i^e_{ds}(k)}{T_s} - \frac{R_s i^e_{ds}(k)}{L_\sigma} + \frac{\omega_e L_\sigma i^e_{qs}(k)}{L_\sigma} \tag{B3}$$

$$C_4 = -\frac{i^e_{qs}(k)}{T_s} - \frac{R_s i^e_{qs}(k)}{L_\sigma} - \frac{\omega_e L_s i^e_{ds}(k)}{L_\sigma} \tag{B4}$$

$$D_1 = -\frac{i^e_{qs}(k)}{T_s} + \frac{v^e_{qs}(k)}{L_\sigma} \tag{B5}$$

$$D_2 = \frac{i^e_{ds}(k)}{T_s} - \frac{v^e_{ds}(k)}{L_\sigma} \tag{B6}$$

$$D_3 = \frac{i^e_{qs}(k)}{T_s} + \frac{R_s i^e_{qs}(k)}{L_\sigma} + \frac{\omega_e L_s i^e_{ds}(k)}{L_\sigma} \tag{B7}$$

$$D_4 = -\frac{i^e_{ds}(k)}{T_s} - \frac{R_s i^e_{ds}(k)}{L_\sigma} + \frac{\omega_e L_\sigma i^e_{qs}(k)}{L_\sigma}. \tag{B8}$$

References

[1] T. Keim, "Electrolytics and film capacitors continue to evolve," *IEEE Power Electron. Mag.*, vol. 5, no. 1, pp. 12–16, Mar. 2018.

[2] S. H. Kim and J. K. Seok, "Induction motor control with small DC-link capacitor inverter fed by three-phase diode front-end rectifiers," *IEEE Trans. Power Electron.*, vol. 30, no. 5, pp. 2713–2720, May 2015.

[3] X. Pan, A. Ghoshal, Y. Liu, Q. Xu, and A. K. Rathore, "Hybrid-modulation-based bidirectional electrolytic capacitor-less three-phase inverter for fuel cell vehicles: analysis, design, and experimental results," *IEEE Trans. Power Electron.*, vol. 33, no. 5, pp. 4167–4180, May 2018.

[4] S. Singh and B. Singh, "Control of three phase inverter for AC motor drive with small DC-link capacitor fed by single phase AC source," *IEEE Trans. Ind. Appl.*, vol. 48, no. 2, pp. 832–838, Mar./Apr. 2012.

[5] N. Mohan, T. M. Undeland, and W. P. Robbins, *Power Electronics: Converters, Applications, and Design*. New York, NY, USA: Wiley, 1995.

[6] K. Inazuma, H. Utsugi, K. Ohishi, and H. Haga, "High-power-factor single-phase diode rectifier driven by repetitively controlled IPM motor," *IEEE Trans. Ind. Electron.*, vol. 60, no. 10, pp. 4427–4437, Oct. 2013.

[7] H. S. Jung, S. J. Chee, S. K. Sul, Y. J. Park, H. S. Park, and W. K. Kim, "Control of three phase inverter for AC motor drive with small DC-link capacitor fed by single phase AC source," *IEEE Trans. Ind. Appl.*, vol. 50, no. 2, pp. 1074–1081, Mar./Apr. 2014.

[8] Y. Son and J. I. Ha, "Direct power control of a three-phase inverter for grid input current shaping of a single-phase diode rectifier with a small DC-link capacitor," *IEEE Trans. Power Electron*., vol. 30, no. 7, pp. 3794–3803, Jul. 2015.

[9] X. Xiao, S. Zhang, Y. Ding, and Y. Song, "Control method of PMSM driving system with small DC-link capacitor," in *Proc. IEEE Energy Convers. Congr. Expo.*, 2017, pp. 1925–1931.

[10] B. G. Kwak and J. K. Seok, "Three-phase inverter control for ac motor drives with small dc-link capacitor fed by dingle-phase diode rectifier," in *Proc. IEEE Energy Convers. Congr. Expo.*, 2018, pp. 6938–6988.

[11] Altivar 21 User's Manual. Schneider Electric Industries S.A.S., 2006.

[12] W. Shireen, M. S. Arefeen, and D. Figoli, "Controlling multiple motors utilizing a single DSP controller," *IEEE Trans. Power Electron*., vol. 18, no. 1, pp. 124–130, Jan. 2003.

[13] J. L. Willems, "A new interpretation of the Akagi-Nabae power components of nonsinusoidal three-phase situations," *IEEE Trans. Instrum. Meas.*, vol. 41, no. 4, pp. 523–527, Aug. 1992.

[14] J. Afonso, M. J. S. Freitas, and J. Martins, "P-Q theory power components calculations," in *Proc. IEEE Ind. Electron. Conf.*, 2003, pp. 385–390.

[15] D. W. Novotny and T. A. Lipo, *Vector Control and Dynamics of AC Drives*. London, U.K.: Oxford Univ. Press, 1996.

ByungGil Kwak received the B.S. and M.S. degrees from Yeungnam University, Gyeongsan, South Korea, in 2015 and 2017, respectively.

He is currently with Aero Mechanical R&D Center, Hanwha Aerospace Corp., South Korea. His research interests include high-performance electrical machine drives.

Jeong-Heum Um received the B.S. degree in electrical engineering in 2017 from Yeungnam University, Gyeongsan, South Korea , where he is currently working toward the combined the M.S./Ph.D. degree in electrical engineering.

His current research interests include high performance electrical machine drives, power electronics for electrical machine control, and wireless power transfer system design for battery charging.

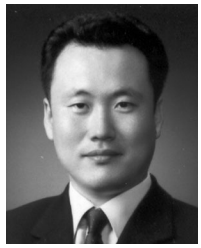

Jul-Ki Seok (S'94–M'98–SM'09) received the B.S., M.S., and Ph.D. degrees from Seoul National University, Seoul, South Korea, in 1992, 1994, and 1998, respectively, all in electrical engineering.

From 1998 to 2001, he was a Senior Engineer with the Production Engineering Center, Samsung Electronics, Suwon, South Korea. Since 2001, he has been a member of the Faculty of the School of Electrical Engineering, Yeungnam University, Gyeongsan, South Korea, where he is currently a Professor. His research interest includes motor drives and power converter control.

Dr. Seok was the recipient of the 2014 IEEE TRANSACTIONS ON INDUSTRY APPLICATIONS Second Place Prize Paper Award and is a Secretary of the IEEE Industry Applications Society Industrial Drives Committee.